Rapid Communications | Editors' Suggestion

Observation of interlayer excitons in $MoSe_2$ single crystals

Jason Horng,[1] Tineke Stroucken,[2] Long Zhang,[1] Eunice Y. Paik,[1] Hui Deng,[1] and Stephan W. Koch[2]
[1]*Physics Department, University of Michigan, 450 Church Street, Ann Arbor, Michigan 48109-2122, USA*
[2]*Department of Physics and Material Sciences Center, Philipps University Marburg, Renthof 5, D-35032 Marburg, Germany*

(Received 12 December 2017; revised manuscript received 13 May 2018; published 7 June 2018)

Interlayer excitons with direct optical transitions are observed coexisting with intralayer excitons in the same K valleys in bilayer, few-layer, and bulk $MoSe_2$ single crystals by confocal reflection contrast spectroscopy. Quantitative analysis using the Dirac-Bloch equations provides unambiguous state assignment of all the measured resonances. The interlayer excitons in bilayer $MoSe_2$ have a large binding energy of 153 meV and a narrow linewidth of 20 meV. Their spectral weight is comparable to the commonly studied higher-order intralayer excitons. At the same time, the interlayer excitons are characterized by distinct transition energies and permanent dipole moments, providing a promising high temperature and optically accessible platform for dipolar exciton physics.

DOI: 10.1103/PhysRevB.97.241404

The basic understanding of spatially direct semiconductor excitons dates back to the 1930s [1,2], where an exciton in a single crystal has been described as a Coulomb bound pair of an electron and a hole that spatially overlap. In heterostructures, spatially indirect excitons can be formed when electrons and holes are separated into neighboring quantum wells by a different material that forms a potential barrier, such as in coupled GaAs quantum wells [3,4]. More recently, spatially indirect excitons are also observed in stacked van der Waals crystals (vdWcs), where the electron and hole are separated into different band minima in different layers [5–12]. Compared to spatially direct excitons, these indirect excitons feature a long radiative lifetime and strong dipole-dipole interactions, but smaller binding energy and greatly reduced oscillator strength.

Here, we report a different type of spatially indirect exciton formed in multilayer single crystals of $MoSe_2$, featuring large binding energy and oscillator strength. These meta-stable interlayer excitons are formed between an electron and hole confined to neighboring molecular layers, albeit in a single crystal and at a higher energy than the coexisting, usual intralayer excitons. Mono-, bi-, tri-, and few-layer up to bulk crystals on the same substrate are studied systematically by confocal reflection contrast spectroscopy and bilayer results are presented with and without encapsulation. The experimental spectra are analyzed by numerically solving the coupled microscopic gap and Dirac-Bloch equations [13,14]. For all structures, the agreement between the theory and experiment is fully quantitative and allows for an unambiguous state assignment.

The identification of such interlayer excitons enriches our basic understanding of the optical and electrical properties of van der Waals crystals. Furthermore, compared to other types of indirect excitons, these single-crystalline interlayer excitons feature much larger exciton binding energies and oscillator strength, both of which can be tuned with external fields, promising a new platform for nonequilibrium many-body physics.

In Fig. 1(a), we schematically show the real-space configuration of the interlayer exciton in a $MoSe_2$ bilayer. Even though the transition from a direct to indirect gap in most vdWc multilayer structures already occurs for the bilayer, the direct gap at the K points of the Brillioun zone is preserved even in the bulk limit, with a dispersion that is flat along the K-H direction [15]. This flat dispersion indicates that the quasiparticles near the K points can be considered as effectively two-dimensional, and are strongly confined within individual layers, with the potential to build bound interlayer excitons even in multilayer structures consisting of identical monolayers.

In Fig. 1(b), we show the band and spin configuration for the noninteracting band structure around the K^+ point in an A-B stacked $MoSe_2$ bilayer. At each K point, the non interacting band structure is composed of the spin-split valence and conduction bands of layer 1 and a mirror identical copy with reversed spin ordering of layer 2 [16]. Consequently, dipole allowed intralayer excitons corresponding to the A series in $MoSe_2$ are formed by an electron in the lowest conduction band and a hole in the highest valence band, whereas the correspondent interlayer exciton uses the upper spin-split conduction band [see arrows in Fig. 1(b)]. Thus, the optical selection rules for the interlayer excitons exhibit similar symmetry properties as those for the intralayer excitons with the difference that the spin-valley selectivity in a monolayer is replaced by spin-layer selectivity for the excitation with circular polarized light.

To experimentally identify interlayer excitons in vdWc multilayers, we perform confocal reflection spectroscopy at 5 K to study the bound electron-hole pairs on $MoSe_2$ flakes with a spatial resolution of 2 μm. Signals from the sample were normalized against a point on the nearby substrate to produce reflection contrast. The first sample A consists of hexagonal boron nitride (hBN) -encapsulated monolayer and bilayer $MoSe_2$ regions. The measured reflection contrast spectrum (R/R_0) for the monolayer region on this sample is shown as a black curve in Fig. 2(a), where R and R_0 are reflection spectra taken from the sample and substrate area, respectively. A typical spectrum of monolayer $MoSe_2$ was observed with reflection peaks corresponding to the A_{1s} (1642 meV) and

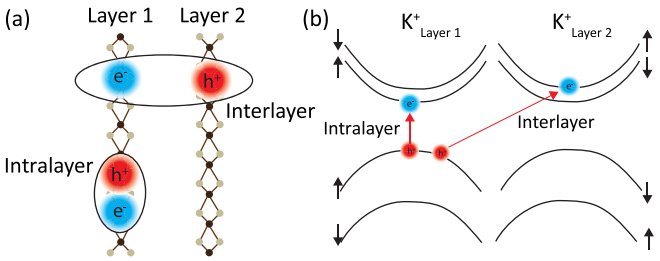

FIG. 1. Schematic illustration of inter- and intralayer excitons in transition-metal-dichalcogenide multilayers. (a) Real-space representation of different species of excitons. Interlayer excitons consist of an electron and a hole in different layers, while the intralayer exciton consists of an electron and a hole in the same layer. (b) k-space and spin configuration for optically bright interlayer and intralayer excitons. The arrows indicate the dipole allowed transitions at the K point of the joint Brillouin zone corresponding to the A-exciton series. At the K^+ points, the layer indices are reversed.

B_{1s} (1839 meV) excitons. Due to the sharp linewidth resulting from the hBN encapsulation, we can also identify the excited excitons A_{2s} at 1793 meV and B_{2s} at 2000 meV, both with much smaller oscillator strengths relative to the $1s$ states. Because of the rapid decrease of spectral weight with increasing quantum number and interference between different species of excitons, we cannot resolve the $3s$,$4s$, ... exciton states experimentally.

The corresponding optical spectrum in the encapsulated bilayer region is shown in Fig. 2(b). The bilayer spectrum has somewhat broader A_{1s} and B_{1s} resonances and we note a redshift of the dominant A_{1s} resonance of 23 meV and a small blueshift of the B_{1s} resonance of 7 meV, respectively. Strikingly, we also observe two additional peaks above the A_{1s} transition at 1711 and 1741 meV with similar oscillator strength, and a weak spectral feature at 1973 meV. Naively, one could try to assign the two peaks above the A_{1s} resonance to the A_{2s} and A_{3s} exciton resonances that are redshifted by the presence of the second layer. However, this assignment is unreasonable due to the similar oscillator strength of the two observed peaks.

To understand the physical origin of the observed features, we employ the theoretical framework that combines an electrostatic model for the Coulomb interaction potential in an anisotropic medium, i.e., the gap equations to determine the interacting gap, and the Dirac-Bloch equations (DBEs) to compute the linear optical response [13]. Within this model, the electronic and optical properties around the K points of the multilayer structures are treated by considering the symmetry induced spin locking of the individual layers. Treating the Hamiltonian of the isolated monolayer within an effective four-band model [17], screening of the bands under consideration is included dynamically, whereas screening of all remaining bands and the dielectric environment is contained in the Coulomb matrix element. The material parameters used are listed in Ref. [18]. This model is based on the observation that the direct gap at the K points, which contributes dominantly to the optical absorption, is preserved while increasing the number of layers from a monolayer to bulk [15]. At the K points, the out-of-plane effective masses of the valence and conduction bands are typically much larger than those in the in-plane directions. Consequently, the out-of-plane component of the kinetic energy can be neglected and the quasiparticles at the K points can be considered as quasi-two-dimensional, well confined within the layers. These assumptions are strongly supported by recent angle-resolved photoemission spectroscopy measurements, which have revealed the two-dimensional nature of the bands at the K point of the Brillouin zone [19].

The theory predicts the resonance positions $A_{1s} = 1629$ meV and $A_{2s} = 1796$ meV in the presence of a small carrier density of $n = 1.3 \times 10^9/\text{cm}^2$ at zero temperature. The computed optical spectrum for the encapsulated monolayer is plotted in Fig. 2(a) for comparison with the experiment. In the numerical evaluations, we introduced a phenomenological linewidth with full width at half maximum (FWHM) of 4 meV for the A_{1s}, 30 meV for other A-exciton resonances, and 40 meV for the B series. The calculation agrees well with the experimentally observed peaks in energy as well as oscillator strengths, allowing for an unambiguous state assignment of the monolayer excitons.

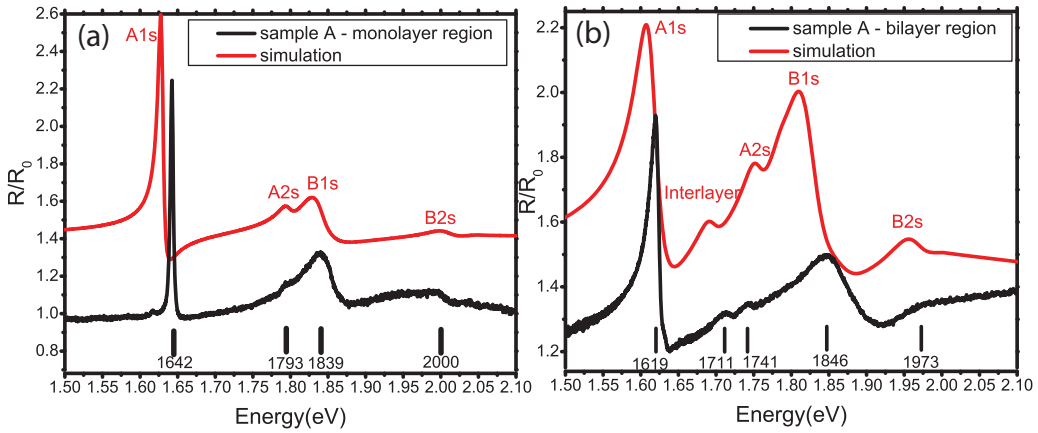

FIG. 2. Measured (black curve) and simulated (red curve) reflection contrast spectra $[R/R_0(E)]$ from the encapsulated monolayer [in (a)] and bilayer [in(b)] regions of sample A, where $R(E)$ and $R_0(E)$ are reflection spectra from the sample and substrate area, respectively. Comparing experiment and theory, we assign the peaks from low to high energy as A_{1s}, A_{2s}, B_{1s}, and B_{2s} for the intralayer excitons and identify the new peak at 1711 meV in the bilayer as the interlayer A_{1s}^{inter} exciton. All simulated spectra have been shifted for better visibility.

Next, we apply the combined gap and DBEs to compute the linear optical response for bilayer $MoSe_2$, using the same parameters for the noninteracting band structure as for the monolayer. As long as one considers only the intralayer contributions, the Elliot formula [20] for an arbitrary layer within the multilayer structure is formally identical to that of a monolayer. However, quantitatively, the intralayer contributions are modified via their dependence on the detailed Coulomb matrix elements which are modified by the presence of both the substrate and the other layers. As a result, each layer in a multilayer configuration experiences a different dielectric environment, generally leading to an intrinsic inhomogeneous broadening of the resonances due to the slightly different contributions from the individual layers. However, for an inversion symmetric bilayer, e.g., a suspended or encapsulated system, both layers are equivalent and resonances corresponding to different intralayer excitons should be degenerate, and thus do not give rise to *additional* resonances. For the encapsulated bilayer configuration at zero temperature and carrier density, we theoretically find the lowest s-type intralayer resonances at $A_{1s} = 1624$ meV, $A_{2s} = 1759$ meV, and $A_{3s} = 1795$ meV, with a relative oscillator strength of 1, 1/5.7, 1/16.3, respectively. Whereas the shift of the A_{2s} exciton resonance agrees with the experimental observations within an accuracy of 10%, the resonance positions and oscillator strengths of the $2s$ and $3s$ intralayer states do not match the experimental data, showing that these states are not responsible for the experimentally observed features.

In addition to the intralayer interactions, the theory predicts that the Coulomb attraction between electrons and holes in adjacent layers should give rise to additional bound interlayer excitons. For the encapsulated bilayer configuration, we find a binding energy of $E^{\text{inter}}_{\text{A}1s} = 153$ meV for the interlayer exciton, only 27% less than the binding energy of $E^{\text{intra}}_{\text{A}1s} = 209$ meV for the lowest intralayer exciton. We find the lowest interlayer exciton at $E^{\text{inter}}_{1s} = 1700$ meV, between the $1s$ and $2s$ resonances of the intralayer exciton. To determine the relative oscillator strength, we estimate the dipole matrix element for the interlayer transition from the d-type Mo orbital centered around the central z positions of the adjacent layers, giving $|\boldsymbol{p}^{n,n\pm1}_{cv}|^2/|\boldsymbol{p}^{n,n}_{cv}|^2 \approx 0.2$. The resulting simulated spectrum for the encapsulated bilayer is shown in Fig. 2(b). A phenomenological broadening (FWHM) of 30 and 50 meV for the A and B series, respectively, have been included in the calculations. The results show quantitative agreement between theory and experiment, therefore we assign the 1741 and 1711 meV peaks as A_{2s} exciton and A-interlayer exciton, respectively.

To further support our interpretation based on interlayer exciton states, we study the influence of thickness on the resonance position and oscillator strength in $MoSe_2$ multilayer systems. We prepare sample B, consisting of $MoSe_2$ monolayer, bilayer, trilayer, quadlayer, and multilayers on a sapphire substrate. In Fig. 3(a), we show the measured reflection contrast for various sample thicknesses. Aside from the two main features around 1625 meV(A_{1s}) and 1875 meV(B_{1s}), we also observed the interlayer peak (1711 meV, blue dot) and A_{2s} shoulder ($\sim$1772 meV, green dot) in the bilayer spectrum. The bulk intralayer species A_{1s} and B_{1s} also redshift about 27 and 15 meV, respectively, from bilayer samples, whereas

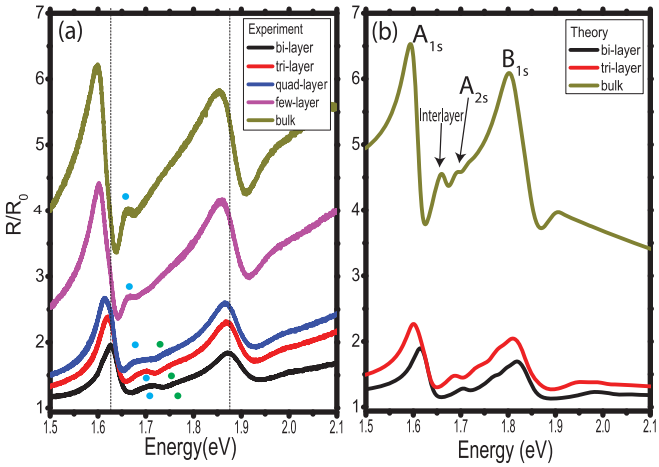

FIG. 3. (a) Thickness dependence of experimental linear optical spectra on sample B. The interlayer exciton resonances are shown as red arrows and show redshift and linewidth narrow as the sample approaches bulk limit. (b) Simulated optical spectra for the corresponding sample thickness.

the observed A interlayer shows a rather strong redshift of 47 meV as it approaches the bulk limit due to increasing dielectric screening. Similar to the monolayer, the shifts result from a simultaneous redshift of the interacting gap and exciton binding energy due to increasing dielectric screening. As can be recognized, the interlayer exciton becomes more apparent in the bulk limit. Apart from the narrower linewidth (35 meV in bilayer and 21 meV in bulk), which is expected due to reduced inhomogeneous broadening arising from the $MoSe_2$ surfaces, the reason for this is the relative oscillator strength. Whereas intralayer contributions increase linearly with the number of layers, the number of next neighbors and therewith the interlayer contributions increase as $2(N-1)$, thus doubling the relative oscillator strength $\Gamma^{\text{inter}}/\Gamma^{\text{intra}}$ going from bilayer to bulk. The same DBE calculations are performed to predict the linear optical response for numbers of layers and are plotted in Fig. 3(b). For the A-exciton series, we find good agreement with the experimental data in terms of both exciton resonance energies and oscillator strengths.

At last, we compare the measured spectra of bilayer $MoSe_2$ with and without hBN encapsulation [Fig. 4(a)]. The encapsulated sample is from sample A [bilayer in Fig. 2(b)] and the nonencapsulated sample is from sample B [bilayer in Fig. 3(a)]. A direct observation is that both the intralayer and interlayer exciton peaks become sharper upon encapsulation. Recently, there are studies [21,22] showing the hBN encapsulation provides a clean platform for high quality monolayer transition metal dichalcogenide crystals (TMDCs) with narrow excitonic linewidth comparable with the theoretical radiative broadening limit. We show that the encapsulation technique can also be applied to bilayer $MoSe_2$ for creating high quality samples. The intralayer exciton linewidth narrowing (from 46 to 20 meV for the A_{1s} state) can be explained by reduced inhomogeneity with hBN interfaces as well as a more symmetric dielectric screening provided by hBN encapsulation, which removes the energy difference between intralayer excitons dwelling in the

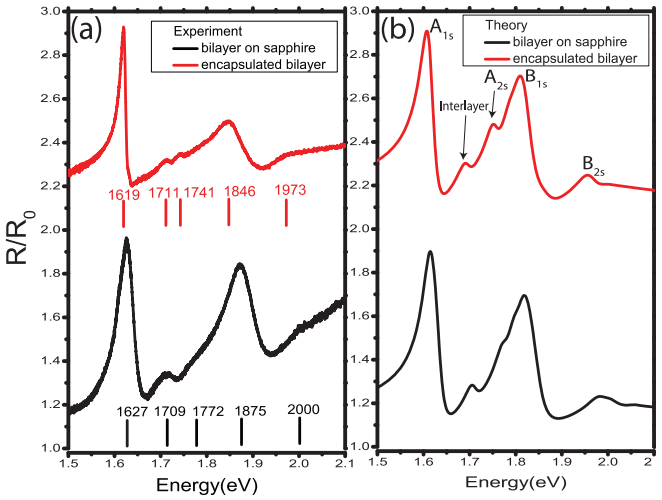

FIG. 4. (a) Comparison between optical spectra of the $MoSe_2$ bilayer with hBN encapsulation (red curve) and without hBN encapsulation (black curve). The $MoSe_2$ bilayer with hBN encapsulation shows a significant linewidth narrowing in both intralayer and interlayer excitonic transitions due to symmetric dielectric screening and a clean environment. (b) Corresponding simulated optical spectra showing the theory is able to capture the dielectric screening effects on different exciton species.

top and bottom layers. The observed interlayer exciton also exhibits linewidth narrowing from 35 to 19 meV, enabling us to identify the interlayer peak unambiguously. Note that the interlayer exciton in the current work shows a narrower linewidth and a much larger oscillator strength than those observed in TMDC heterojunctions, which typically have linewidth around 50–100 meV and oscillator strength 1/100 of the A_{1s} state [23–25].

In summary, the strongly confined quasiparticles in vdWc layered semiconductors provide an interesting platform to form bound interlayer excitons. Through a comparison between experimental and theoretical studies on linear optical spectra, we clearly identify the A-interlayer exciton in few-layer $MoSe_2$ systems. We first demonstrate that our DBE model reproduces the experimental monolayer $MoSe_2$ optical spectrum with a quantitative match and apply the same method to the few-layer $MoSe_2$ situation. The identification of interlayer excitons in layered single crystals substantiates the two-dimensional nature of electron behaviors, and is of crucial importance for the correct understanding of several anomalous phenomena observed in multilayer TMDCs. Therefore our work is an essential step toward understanding the interlayer microscopic interactions in van der Waals materials.

The observed interlayer excitons also provide a promising platform for many-body physics. On one hand, similar to indirect excitons in heterostructures, the interlayer excitons have a permanent, aligned dipole moment that leads to long-range dipole-dipole interactions and a wide range of associated quantum many-body phenomena [26–31]. On the other hand, being direct band gap and single crystalline, they allow narrower linewidth, strong exciton binding energy, a larger oscillator strength, and ease of fabrication.

We have measured an interlayer exciton linewidth of 19 meV, which is comparable to that of intralayer excitons and indirect excitons in vdWc heterostructures with hBN encapsulation [10–12,32]. Due to their permanent dipole moment, indirect excitons in conventional semiconductor heterostructures are sensitive to local electronic disorders including those at the internal interfaces of the heterostructures. In contrast, interlayer excitons in monocrystalline vdWCs do not experience internal interfaces. Furthermore, the external crystal surfaces can be very effectively passivated by hBN layers. These near ideal structural conditions reflect themselves in the measured narrow linewidth.

The interlayer excitons maintain a relatively large exciton binding energy, 153 meV in $MoSe_2$, due to the close proximity of the neighboring molecular layers. Therefore, they may allow dipolar exciton studies at the presence of relatively high doping densities and temperatures. The interlayer excitons also correspond to a direct band-gap optical transition with a much larger oscillator strength compared to those in heterostructures. This will enable convenient optical access to the system and potentially powerful cavity effects [33,34]. Additional controls, such as a bias field, can be used to reduce the oscillator strength and lower the exciton transition energy to obtain longer lifetimes when desired [27,35,36].

Lastly, bilayer and fewlayer vdWcs are easier to fabricate than heterostructures and do not suffer from lattice mismatch or angle rotation between the constituting lattices. Future work will improve the crystal quality for narrower linewidths and will integrate electrical controls to tune and optimize the interactions, oscillator strength, and lifetime of these excitons.

The experimental work in Michigan is supported by the United States Army Research Office MURI award W911NF-17-1-0312. The Marburg part of the work is a project of the Collaborative Research Center SFB 1083 funded by the Deutsche Forschungsgemeinschaft.

[1] J. Frenkel, Phys. Rev. **37**, 17 (1931).
[2] G. H. Wannier, Phys. Rev. **52**, 191 (1937).
[3] M. Colocci, M. Gurioli, A. Vinattieri, F. Fermi, C. Deparis, J. Massies, and G. Neu, Europhys. Lett. **12**, 417 (1990).
[4] L. V. Butov, A. Zrenner, G. Abstreiter, G. Böhm, and G. Weimann, Phys. Rev. Lett. **73**, 304 (1994).
[5] A. K. Geim and I. V. Grigorieva, Nature (London) **499**, 419 (2013).
[6] D. Jariwala, T. J. Marks, and M. C. Hersam, Nat. Mater. **16**, 170 (2016).
[7] P. Rivera, J. R. Schaibley, A. M. Jones, J. S. Ross, S. Wu, G. Aivazian, P. Klement, K. Seyler, G. Clark, N. J. Ghimire, J. Yan, D. G. Mandrus, W. Yao, and X. Xu, Nat. Commun. **6**, 6242 (2015).
[8] Philipp Nagler, Gerd Plechinger, Mariana V. Ballottin, Anatolie Mitioglu, Sebastian Meier, Nicola Paradiso, Christoph Strunk, Alexey Chernikov, Peter C. M. Christianen, Christian Schüller, and Tobias Korn, 2D Mater. **4**, 025112 (2017).
[9] X. Zhu, N. R. Monahan, Z. Gong, H. Zhu, K. W. Williams, and C. A. Nelson, J. Am. Chem. Soc. **137**, 8313 (2015).

[10] J. R. Schaibley, P. Rivera, H. Yu, K. L. Seyler, J. Yan, D. G. Mandrus, T. Taniguchi, K. Watanabe, W. Yao, and X. Xu, Nat. Commun. **7**, 13747 (2016).

[11] J. S. Ross, P. Rivera, J. Schaibley, E. Lee-Wong, H. Yu, T. Taniguchi, K. Watanabe, J. Yan, D. Mandrus, D. Cobden, W. Yao, and X. Xu, Nano Lett. **17**, 638 (2017).

[12] Z. Wang, Y.-H. Chiu, K. Honz, K. F. Mak, and J. Shan, Nano Lett. **18**, 137 (2018).

[13] L. Meckbach, T. Stroucken, and S. W. Koch, Phys. Rev. B **97**, 035425 (2018).

[14] L. Meckbach, T. Stroucken, and S. W. Koch, Appl. Phys. Lett. **112**, 061104 (2018); T. Stroucken and S. W. Koch, in *Optical Properties of Graphene*, edited by R. Binder (World Scientific Publishing, Singapore, 2017), Chap. 2, pp. 43–84.

[15] M. Ye, D. Winslow, D. Zhang, R. Pandey, and Y. K. Yap, Photonics **2**, 288 (2015).

[16] A. M. Jones, H. Yu, J. S. Ross, P. Klement, N. J. Ghimire, J. Yan, D. G. Mandrus, W. Yao, and X. Xu, Nat. Phys. **10**, 130 (2014).

[17] D. Xiao, G.-B. Liu, W. Feng, X. Xu, and W. Yao, Phys. Rev. Lett. **108**, 196802 (2012).

[18] In the massive Dirac-Fermion for $MoSe_2$ layers, we use the following parameters: energy gap $\Delta = 1.47$ eV, effetive hopping matrix element $t = 0.94$ eV, lattice constant $a = 3.313$ Å, and the spin splitting of valence and conduction band $2\lambda_v = 0.18$ eV and $2\lambda_c = 0.02$ eV, as given in Ref. [17]. The in-plane and out-of-plane background dielectric constants are 3.36 and 5.16, respectively. Furthermore, we use a natural layer-to-layer distance of $D = 6.5$ Å and an effective thickness parameter characterizing the finite extension of the Mo-d orbitals in out-of-plane direction of 5 Å.

[19] J. M. Riley, F. Mazzola, M. Dendzik, M. Michiardi, T. Takayama, L. Bawden, C. Granerød, M. Leandersson, T. Balasubramanian, M. Hoesch, T. K. Kim, H. Takagi, W. Meevasana, P. Hofmann, M. S. Bahramy, J. W. Wells, and P. D. C. King, Nat. Phys. **10**, 835 (2014).

[20] H. Haug and S. W. Koch, *Quantum Theory of the Optical and Electronic Properties of Semiconductors*, 5th ed. (World Scientific, Singapore, 2009).

[21] F. Cadiz, E. Courtade, C. Robert, G. Wang, Y. Shen, H. Cai, T. Taniguchi, K. Watanabe, H. Carrere, D. Lagarde, M. Manca, T. Amand, P. Renucci, S. Tongay, X. Marie, and B. Urbaszek, Phys. Rev. X **7**, 021026 (2017).

[22] O. A. Ajayi, J. V. Ardelean, G. D. Shepard, J. Wang, A. Antony, T. Taniguchi, K. Watanabe, T. F. Heinz, S. Strauf, X.-Y. Zhu, and J. C. Hone, 2D Mater. **4**, 031011 (2017).

[23] M. Förg, L. Colombier, R. K. Patel, J. Lindlau, A. D. Mohite, H. Yamaguchi, D. Hunger, and A. Högele, arXiv:1710.00990.

[24] B. Miller, A. Steinhoff, B. Pano, J. Klein, F. Jahnke, A. Holleitner, and U. Wurstbauer, Nano Lett. **17**, 5229 (2017).

[25] M. Baranowski, A. Surrente, L. Klopotowski, J. M. Urban, N. Zhang, D. K. Maude, K. Wiwatowski, S. Mackowski, Y. C. Kung, D. Dumcenco, A. Kis, and P. Plochocka, Nano Lett. **17**, 6360 (2017).

[26] M. M. Fogler, L. V. Butov, and K. S. Novoselov, Nat. Commun. **5**, 4555 (2014).

[27] E. V. Calman,M. M. Fogler,L. V. Butov, S. Hu, A. Mishchenko, and A. K. Geim, Nat. Commun. **9**,1895 (2018).

[28] Mathieu Alloing, Mussie Beian, Maciej Lewenstein, David Fuster, Yolanda González, Luisa González, Roland Combescot, Monique Combescot, and François Dubin, Europhys. Lett. **107**, 10012 (2014).

[29] Monique Combescot, Roland Combescot, and François Dubin, Rep. Prog. Phys. **80**, 066501 (2017).

[30] J.-J. Su and A. H. MacDonald, Phys. Rev. B **95**, 045416 (2017).

[31] O. L. Berman and R. Y. Kezerashvili, Phys. Rev. B **96**, 094502 (2017).

[32] A. Ciarrocchi, D. Unuchek, A. Avsar, K. Watanabe, T. Taniguchi, and A. Kis, arXiv:1803.06405.

[33] H. Deng, H. Haug, and Y. Yamamoto, Rev. Mod. Phys. **82**, 1489 (2010).

[34] I. Carusotto and C. Ciuti, Rev. Mod. Phys. **85**, 299 (2013).

[35] Y.-H. Zhao, F. Yang, J. Wang, H. Guo, and W. Ji, Sci. Rep. **5**, 8356 (2015).

[36] D. Lloyd, X. Liu, J. W. Christopher, L. Cantley, A. Wadehra, B. L. Kim, B. B. Goldberg, A. K. Swan, and J. S. Bunch, Nano Lett. **16**, 5836 (2016).